

1 **Autism in a dish: ES cell models of autism with copy number**  
2 **variations reveal cell-type-specific vulnerability**

3

4 Jun Nomura<sup>1,2</sup>, Amila Zuko<sup>1,3\*</sup>, Keiko Kishimoto<sup>1\*</sup>, Hiroaki Mutsumine<sup>1</sup>, Kazumi  
5 Fukatsu<sup>1</sup>, Yoshiko Nomura<sup>1</sup>, Xiaoxi Liu<sup>1</sup>, Nobuhiro Nakai<sup>1,2</sup>, ES library team<sup>\*\*</sup>, Eiki  
6 Takahashi<sup>1</sup>, Tsukasa Kouno<sup>4</sup>, Jay W. Shin<sup>4</sup>, Toru Takumi<sup>1,2,5</sup>

7

8 \* These authors contributed equally to this work.

9 \*\*ES library team: Chika Maeda<sup>1</sup>, Yuriko Kusakari<sup>1</sup>, Takashi Arai<sup>1</sup>, Ikue Shibasaki<sup>1</sup>,  
10 Ayaka Homma<sup>1</sup>, Kaori Yanaka<sup>1</sup>, Keigo Matsuno<sup>1</sup>, Emilia Bergoglio<sup>1</sup>, Yuki Sakai<sup>1</sup>,  
11 Qalam Eusuf<sup>1</sup>, Mizuki Seki<sup>1</sup>, Roberta T Fresia<sup>1</sup>, Sawako Furukawa<sup>1</sup>, Shigehiro Kuraku<sup>5</sup>,  
12 Piero Carninci<sup>4</sup>

13

14 <sup>1</sup> RIKEN Brain Science Institute, Wako, Saitama 351-0198, Japan

15 <sup>2</sup> Department of Physiology and Cell Biology, Kobe University School of Medicine,  
16 Chuo, Kobe 650-0017, Japan.

17 <sup>3</sup> Department of Molecular Neurobiology, Donders Institute for Brain, Cognition and  
18 Behaviour and Faculty of Science, Radboud University, Nijmegen 6525JA,  
19 Netherlands

20 <sup>4</sup> RIKEN Center for Integrative Medical Sciences, Tsurumi, Yokohama 230-0045,  
21 Japan

22 <sup>5</sup> RIKEN Center for Biosystems Dynamics Research, Chuo, Kobe 650-0047, Japan

23 **SUMMARY**

24 Human genetics has identified numerous single nucleotide variations (SNVs) and copy  
25 number variations (CNVs) associated with autism spectrum disorders (ASD) and other  
26 psychiatric disorders. However, the lack of standardized biological resources impedes  
27 understanding of the common pathophysiology of ASD. Here, using next-generation  
28 chromosome engineering based on the CRISPR/Cas9 system, we established a  
29 biological resource including 65 genetically modified mouse embryonic stem cell  
30 (mESC) lines as genetic models of human SNVs and CNVs. To illustrate cell-type and  
31 CNV specific molecular features of ASD, we performed single-cell RNA sequencing  
32 (37,397 cells in total), morphological, and physiological analyses using 12  
33 representative cell lines with CNVs highly associated with ASD. These results uncover  
34 gene ontology (GO) terms, canonical pathways, upstream regulators, and related  
35 neuropsychiatric disorders in a cell-type and CNV specific manner.

36

## 37 INTRODUCTION

38 Autism spectrum disorder (ASD) is a highly heritable neurodevelopmental disorder  
39 characterized by social deficits with restricted interests and repetitive behaviors.  
40 Although considerable heterogeneity of genetics and clinical phenotypes have been  
41 reported in ASD<sup>1</sup>, remarkable advances in sequencing technologies have identified  
42 numerous *de novo* single nucleotide variants (SNVs) and copy number variations  
43 (CNVs) associated with ASD<sup>2-4</sup>. CNVs generally include multiple genes with  
44 regulatory elements such as promoter, enhancer, and repressor in the genome, which  
45 may contribute to the complexity and comorbidity of ASD pathology. Thus, it is ideal  
46 to analyze multiple CNVs in the same experimental platform to identify convergent  
47 pathways and molecular networks implicated in the pathophysiology of ASD. To date,  
48 these human genetic data are archived in web-based databases such as the Simons  
49 Foundation Autism Research Initiative (SFARI) and AutDB to adopt increasing genetic  
50 variants found in patients with ASD<sup>5,6</sup>. These human genetic data have also identified  
51 several CNVs derived from patients with ASD overlapping with those observed in other  
52 neuropsychiatric diseases such as schizophrenia and bipolar disorders<sup>7,8</sup>.

53 Genetic evidence-based biological research is still challenging because of the  
54 lack of standardized bioresources. To overcome these limitations, we developed an  
55 ASD-associated CNV cell bank as a biological resource for ASD using mouse  
56 embryonic stem cells (mESCs) and a next-generation chromosome engineering  
57 technique based on CRISPR/Cas9 system. This unique bioresource includes 65 CNVs  
58 with deletions and duplications covering 58 human chromosome loci and 175  
59 additional vectors targeting these loci. These mESC cell lines provide major benefits as  
60 a biological resource for generating mutant mice, transplantation to living animals, and  
61 blastocyst complementation to assess neural development and morphogenesis of the *in*

62 *vivo* brain environment<sup>9</sup>. Using neural cells derived from 12 representative cell lines

63 we tried to identify the features commonly dysregulated in ASD by applying

64 morphological, physiological, and single-cell transcriptome analyses.

65

## 66 RESULTS

### 67 *Annotation of human CNVs to mouse genomic loci*

68 To develop the ASD-associated CNV cell bank as a comprehensive biological platform  
69 for ASD research (Fig. 1a), we first referred to the SFARI database  
70 (<https://gene.sfari.org/database/human-gene/>) together with published data to survey  
71 ASD-associated CNVs. The SFARI database is a database for ASD by integrating  
72 published human genetic and animal model data. It contains more than 1,000 genes and  
73 2,000 CNVs associated with ASD<sup>6</sup>. Using this database, we first listed 104 ASD-  
74 associated CNVs as candidates for the followed chromosome targeting (Extended Data  
75 Table 1). We analyzed syntenic regions between humans and mice for each CNV. Some  
76 CNVs, 35 out of 104 loci, such as 1q44, 14q11.2, and Xp22.31, were omitted from our  
77 chromosome targeting list because of the low conservation in the mouse genomic  
78 structure (Supplementary Table 1). Other CNVs which are recognized as significant  
79 risk loci across multiple psychiatric disorders have remained in our list, such as 1q21.1,  
80 2p16.3 (*NRXNI*), 3q29, 7q11.23, 8p23.1, 15q11.2, 15q13.3, 16p11.2 (proximal region,  
81 from breakpoint (BP)4 to BP5), 16p13.2, 22q11.21, and 15q11-q13 Prader-Willi  
82 syndrome region (Extended Data Table 2)<sup>7,8,10</sup>. These CNVs contain genes associated  
83 with other psychiatric disorders such as schizophrenia, bipolar disorders, attention-  
84 deficit hyperactivity disorder (ADHD), and intellectual disability (ID). Other major  
85 CNVs, such as 3p26.3, 15q11.2-q13.1, 15q13.3, and 22q11.21, also include multiple  
86 psychiatric risk genes (Extended Data Table 3).

87

88 *Generation of cell models for ASD by using next-generation chromosome*  
89 *engineering*

90 To generate cell models of ASD, we developed next-generation chromosome  
91 engineering using the CRISPR-based genome editing technique. First, we introduced  
92 two CRISPR/Cas9 vectors, pX330<sup>11</sup> with a 20-nucleotide (nt) guide sequence and a  
93 targeting vector with short homology arms (1~2 Kb) into murine C57BL/6J background  
94 ES cells (mESCs), CMTI-2. We introduced the CRISPR/Cas9 pX330 vectors without  
95 a 20-nt target sequence into mESCs as a control cell line. This next-generation  
96 chromosome engineering using a targeting vector together with CRISPR/Cas9 vectors  
97 based on homology-directed repair (HDR) brought ~10% targeting efficiency with low  
98 false positives cells by a diphtheria toxin A (DT-A) fragment as a negative selection  
99 marker (Fig. 1b-d).

100 Using *in silico* and experimentally validated 120 CRISPR vectors and 55  
101 targeting vectors (Supplementary Table 2)<sup>12</sup>, we obtained 65 cell lines, including 58  
102 deletions (one-copy, or null mutation (knockout)), 2 tandem duplication (two-copies),  
103 and 5 duplications (three-copies) (Fig. 1e, Extended Data Tables. 4, 5). Two out of 65  
104 cell lines, mouse chromosome 7 corresponding to human 15q11.2-q13.1 duplication  
105 (paternal or maternal duplication, respectively), were established from mouse  
106 blastocyst by crossing paternally inherited 15q11.2-q13.1 duplication male mice<sup>13</sup> with  
107 C57BL/6J wild-type (WT) female mice or C57BL/6J WT male mice with maternally  
108 inherited 15q11.2-q13.1 female mice<sup>13</sup>, respectively. All cell lines were verified for  
109 targeted deletion or duplication by PCR, and some lines were followed by array  
110 comparative genomic hybridization (aCGH) and Southern blotting analysis.

111 One of the advantages of mESC is its application to generating mouse models.  
112 We developed a mouse model with CNV using a cell line corresponding to human  
113 chromosome 15q13.3. This human locus encompasses two genes, *CHRNA7* and  
114 *OTUD7A*, which are highly conserved in the mouse 7qC locus (Fig. 1b). The targeted

115 15q13.3 heterozygote mESCs were injected into blastocysts, and chimera offspring  
116 mice were generated (Extended Data Figs. 1a, b). The sperms of 60% chimera mice  
117 were then fertilized with C57BL/6J WT egg *in vitro* to produce mice lacking one copy  
118 of the 15q13.3 allele (15q13.3(+/-)). Genotype was confirmed by PCR (Extended Data  
119 Fig. 1c). Using adult cortices, the gene expression in 15q13.3 was assessed by  
120 quantitative real-time RT-PCR (RT-qPCR). The result showed approximately 50%  
121 reduction of *Chrna7* and *Otud7a* in 15q13.3(+/-) mice, respectively (Extended Data Fig.  
122 1d).

123 Using 15q13.3 (+/-) mice, we performed a battery of behavioral tests and  
124 compared the results with previous studies<sup>14,15</sup>. Although 15q13.3(+/-) mice were  
125 healthy and fertile with no gross physical abnormalities, they showed social deficits in  
126 the three-chamber social interaction test, increased startle response to a sudden noise,  
127 and increased body weights in the developmental period, which was observed in human  
128 subjects with 15q13.3 deletion<sup>14</sup>. These results illuminate *Chrna7-Otud7a* genetic  
129 interaction relevant to ASD-like symptoms (Extended Data Fig. 1e-p). This test  
130 successfully narrowed down the critical region for social deficits in the 15q13.3  
131 microdeletion syndrome from 1.5 Mb (from *Chrna7* to *Fan1*) to 0.7 Mb (from *Chrna7*  
132 to *Otud7a*) and demonstrate the significance of mice generated using mESCs for  
133 modelling human psychiatric disorders *in vivo*.

134

### 135 ***Morphological and physiological analyses of cell models with ASD-associated CNV***

136 To analyze biological aspects of ASD-associated CNVs, we selected 12 CNVs as  
137 representatives for the following experiments, duplication of 1q21.1 (MIM: 612475),  
138 deletion of 2p16.3 (MIM: 614332), 3q29 (MIM: 609425), duplication of 7q11.23  
139 (MIM: 613729), deletion of 15q11.2 (MIM: 615656), 15q13.3 (MIM: 612001),

140 16p11.2 (MIM: 611913), 16p13.2 (MIM: 616863), 17p11.2 (MIM: 182290), 17q12  
141 (MIM: 614527), Xq27.3 (MIM: 300624) and, Xq28 (MIM: 312750) (Extended Data  
142 Table 1). These CNVs were selected based on two previous genetic ASD cohorts  
143 studies, *de novo* CNVs from the Simons Simplex Collection (SSC) 2,591 families<sup>16</sup> and  
144 both *de novo* and rare CNVs on ASD risk in multiplex 1,532 families from the Autism  
145 Genetic Resource Exchange (AGRE)<sup>17</sup>. Xq27.3 (*Fmr1*) and Xq28 (*Mecp2*) were  
146 selected as a monogenic cause of syndromic ASD<sup>18</sup>. Genes located in each CNV were  
147 highly conserved in mice (Extended Data Table 6). Targeted deletion or duplication in  
148 these representative CNVs was confirmed by a-CGH (Extended Data Fig. 2) and gene  
149 expression profiles in the targeted loci (Extended Data Table 7).

150 We next differentiated these ES cells into neurons. On day 1 of *in vitro*  
151 differentiation, differentiating neurons were transfected with a green fluorescent  
152 protein (GFP) expression vector and fixed on day 3 to visualize them. Although we  
153 measured axon length, total neurite length ( $\mu\text{m}$ ), and the number of neuronal branches,  
154 we found no significant difference between these mutants and control (Extended Data  
155 Fig. 3a-c). We then assessed neuronal response based on activity-dependent calcium  
156 influx. Differentiated neurons were loaded with the calcium indicator, Fluo-4, and their  
157 intracellular calcium mobilization was measured by application of 25 mM KCl, leading  
158 to membrane depolarization (Extended Data Fig. 3d). One-way ANOVA showed a  
159 significant effect of genotype for response amplitude of the fluorescent intensity, ( $\Delta F/F$ ),  
160  $F(12,185)=5.27$ , ( $p < 0.001$ ). The Bonferroni multiple comparisons test for *post-hoc*  
161 comparisons revealed a significance in 3q29 deletion vs. control cells ( $p < 0.001$ )  
162 (Extended data Fig. 3e). The result is consistent with the previous report using 3q29  
163 deletion model mice, which showed excitatory/inhibitory imbalance derived from



164 increased excitatory neural activity in the cerebral cortex<sup>19</sup>. These results indicate that  
165 the ES cell models could be morphologically and physiologically differentiated.

166

### 167 ***Cell-type-specificity of gene expression and genetic associations with ASD***

168 To reveal cell-type-specific expression of our multiple ASD cell lines, we performed  
169 single-cell RNA-sequencing (scRNA-seq) on the 10x Genomics platform using  
170 differentiated neuronal cells of 12 representative ASD-associated CNVs and a control  
171 mESCs line. We collected 37,397 cells in total, 2,858 cells from control and 34,539  
172 cells from cell models across 12 CNVs. We then visualized all single-cells in a uniform  
173 manifold approximation and projection (UMAP) space to analyze cell-type-specific  
174 features in each cell model with CNV. The cell-type was annotated according to gene  
175 expression of canonical cell-type-specific markers (e.g., *Slc17a6* for glutamatergic  
176 neurons, *Gad1* for GABAergic neurons, *Fabp7* for neural stem cells and immature  
177 astrocytes, *Neurod6* for neural progenitors, *Ifrd1* for microglia, *Pdgfra* for OPC  
178 (oligodendrocyte precursor cell), *Colla1* for endothelial cells, and *Pou5f1* for ES cells)  
179 and we finally identified 17 cell-types in total (Fig. 2a-d, Supplementary Table 3)<sup>20-23</sup>.  
180 The cell-type-specific differentially expressed genes (DEGs) include cortical upper-  
181 layer (2/3) specific glutamatergic neuronal genes such as *Cux2*, *Hap1*, and  
182 *Tmem145*<sup>24,25</sup>. In addition, UMAP revealed two different types of GABAergic neuronal  
183 clusters, one with *Gad1+Sst+Npy+* and the other one with *Gad1+Sst+Npy-*. Both of  
184 these clusters expressed GABAergic marker *Gad1* with a subtype marker *Sst*, which  
185 has been classified as Martinotti cells<sup>26</sup>. Although GABAergic *Npy+* cells are widely  
186 expressed throughout the cortex, Martinotti-like cells co-expressed with *Sst*  
187 (*Sst+Npy+*) are regarded as the most excitable type<sup>27</sup>.

188           The cell type with the annotation was also confirmed by Gene Ontology (GO),  
189   the Kyoto Encyclopedia of Genes and Genomes (KEGG), and Reactome enrichment  
190   analysis (Extended Data Table 8). Brain regions and developmental stages were  
191   determined by cell-type-specific expression enrichment analysis (CSEA) using 300  
192   cluster-specific DEGs (adjusted  $p < 0.001$ )<sup>28</sup>. These neuronal gene sets were mainly  
193   enriched in both cortex and thalamic regions from the early fetal to late infancy period  
194   (Fig. 2e).

195           We also analyzed the interaction between ASD genetic risk factors (SFARI  
196   genes, risk score 1 to 3 plus syndromic genes) and cell-type-specific DEGs (top 300,  
197   adjusted  $p < 0.001$ ) to assess the cell-type-specific contribution to ASD  
198   pathophysiology and pathogenesis (Fig. 2f). Remarkably, the upper-layer specific  
199   glutamatergic neuronal cluster largely overlapped with SFARI ASD risk genes (Fig. 2f,  
200   top rank). The tendency was consistent with a single-cell transcriptome study using  
201   postmortem cortical tissues from autistic individuals<sup>29</sup>. ASD risk genes were also  
202   highly expressed in neural stem and progenitor cells (Fig. 2f, 5th and 6th ranks),  
203   suggesting the pathological primed stage in neural fate<sup>30</sup>. In contrast, the effects of  
204   microglia (1.7%), OPCs (1.3%), and endothelial cells (2.3-1.7%) on ASD pathology  
205   were likely weaker than those of neuronal cells. However, biological evidence supports  
206   the importance of glial cells, and even in endothelial cells in the brain  
207   microenvironment for ASD pathology<sup>31,32</sup>. Indeed, vascular contributions of the  
208   16p11.2 CNV have been recently published<sup>33</sup>.

209

### 210 ***Molecular signatures of cell models with ASD-associated CNVs***

211   Several convergent pathways underlying ASD pathophysiology have been suggested  
212   from studies using lymphoblasts, postmortem brains, and iPSCs from patients with

213 ASD<sup>34-36</sup>. We investigated convergent features of ASD as well as each CNV from GO  
214 and pathway analysis using 12 representative ASD cell models. First, CNV specific  
215 DEGs were analyzed by GO and GO-network analysis. As expected, representative  
216 ASD-associated CNVs were significantly enriched in neuron, transcription, and  
217 translation-associated terms regardless of genotype, consistent with previous studies<sup>2</sup>  
218 (Fig. 2g and Extended Data Table 9). In this enrichment analysis, immune systems were  
219 enriched in the ASD network. They were also repeatedly reported as a risk factor for  
220 ASD and other psychiatric disorders<sup>37</sup>. Interestingly, enrichment terms such as  
221 mitochondria dysfunction, chromatin, and synapse in GO analysis, and mTOR pathway,  
222 ubiquitin pathway, oxidative phosphorylation, and DNA damage in canonical pathway  
223 analysis have also been recognized as dysregulated factors for other psychiatric  
224 disorders<sup>38,39</sup> (Extended Data Fig. 4).

225

### 226 *Cell-type-specific features across cell models with ASD-associated CNVs*

227 To analyze cell-type-specific features in ASD-associated CNVs, we first examined the  
228 gene-disease association based on GWAS. Although neuronal cells were enriched in  
229 both neuropsychiatric and neurological features, GABAergic (*Gad1+Sst+Npy-*) cluster  
230 was especially more remarkable than that of other subtypes (Extended Data Fig. 5). The  
231 pathogenesis of neuropsychiatric disorders, including ASD, is highly associated with  
232 synaptic dysfunctions<sup>40,41</sup>. Thus, we next focused on the genes related to glutamatergic  
233 synapse by analyzing the relationship between glutamatergic cluster-specific genes  
234 (GCG) ( $p < 0.05$  and  $\log_2$ -fold change  $> 0.4$ ) and the SFARI genes. We referred datasets  
235 of postsynaptic density (PSD) complex proteins<sup>42</sup>, and realized that the PSD complex  
236 genes were substantially enriched in glutamatergic cluster (total average 24.0%, 1q21.1  
237 dup, 31.0-32.7%; 2p16.3 del, 12.7-15.0%; 3q29 del, 26.7-27.9%; 7q11.23 dup, 23.7-

238 28.3%; 15q11.2 del, 28.0-29.1%; 15q13.3 del, 22.4-23.8%; 16p11.2 del, 24.7-26.2%;  
239 16p13.2 del, 15.8-27.5%; 17p11.2 del, 21.0-24.8%; 17q12 del, 19.1-22.3%; Xq27.3 del,  
240 24.1-24.8%; Xq28 del, 19.6-24.0%) (Extended Data Fig. 6a).

241 We then assessed the “upstream regulators” that potentially affect the GCG as  
242 their downstream genes by using Ingenuity Pathway Analysis (IPA) (Extended Data  
243 Fig. 6b). Overall, neural development and neuronal function-related genes, such as  
244 *MAPT*, *PSENI*, and *APP* (these are implicated in the etiology of Alzheimer's disease),  
245 *POLG*, a mitochondrial DNA polymerase, *ADORA2A*, an adenosine A(2A) receptor,  
246 *MKNKI*, a MAPK interacting serine/threonine kinase, *RTN4*, a potent neurite  
247 outgrowth inhibitor, *SOD1*, a major cytoplasmic antioxidant enzyme, and *FMRI*, a  
248 negative translational regulator, were highly enriched regardless of cell-type or CNV  
249 associated with ASD. Genes significantly enriched in ASD-associated CNVs, such as  
250 *MAPT*, *FMRI*, *PSENI*, *APP*, *ADORA2A*, *SOD1*, *POLG*, *KMT2A*, *YWHAZ*, *CREBZF*,  
251 *SERPINA1*, and *TP53*, have been reported as ASD risk or susceptible genes.

252 We performed canonical pathway analysis using IPA (Fig. 3a). Of note, three  
253 major translational pathways, EIF2 signaling, regulation of eIF4 and p70S6K signaling,  
254 and mTOR signaling, were enriched through all 12 cell lines containing ASD-  
255 associated CNVs, followed by mitochondria dysfunctions, oxidative phosphorylation,  
256 and protein ubiquitination pathway. These pathways seemed common and convergent  
257 regardless of cell type and psychiatric disorders. The analysis also identified cell-type-  
258 specific enriched pathways, unfolded protein response (UPR) and endoplasmic  
259 reticulum (ER) stress for *Gad1+Sst+Npy+* GABAergic neurons. p53 signaling for non-  
260 neuronal cells such as microglia and endothelial cells. These data indicate that p53, a  
261 tumor suppressor, is involved in the various biological process regardless of the cell-  
262 types<sup>43</sup> and affects non-neuronal cell lineage in ASD-associated CNVs.

263 We then analyzed major targets of ASD such as FMRP, CHD8, WNT- $\beta$  catenin,  
264 and the MAP kinase pathway<sup>44</sup> (Fig. 3b). This analysis found cell-type-specific  
265 pathway regulation; in particular, FMRP target genes were mostly enriched in neuronal  
266 clusters but not in other cell types. Meanwhile, CHD8 target genes were enriched in all  
267 cell types except for endothelial cells, although both FMRP and CHD8 protein are  
268 expressed ubiquitously.

269

270

## 271 **DISCUSSION**

272 This study has established an ASD cell bank in which 65 ASD-associated chromosome  
273 loci were targeted as a standardized platform for ASD research. These targeted CNVs  
274 and genes are highly associated with not only ASD but also other neurodevelopmental  
275 and neuropsychiatric disorders such as schizophrenia and bipolar disorder. Thus, the  
276 cell models developed in this study contribute to the research for multiple  
277 neurodevelopmental and psychiatric disorders. Moreover, the model was established  
278 using multipotent mESCs. Thus, as demonstrated in this study, we can generate mouse  
279 models of ASD containing CNVs of interest by introducing these mESCs into  
280 blastocyst-stage host embryos. It is also possible to differentiate the mESCs into  
281 multiple cell lineages of different tissues or organs *in vitro* as well as three-dimensional  
282 (3D) organoid cultures. In addition, these cell models allow us to perform  
283 transplantation and blastocyst complementation studies<sup>9</sup>. Therefore, our cell models  
284 would be valuable tools for various organogenesis studies with disease modeling *in*  
285 *vivo* and *vitro*.

286 Recent advances in genome editing techniques enable us to generate mutant  
287 animal models faster and efficiently than before. With genome editing tools such as the

288 CRISPR/Cas9 system, gene targeting can be achieved directly in zygotes via  
289 microinjection of genome editing reagents without requiring mutant ES cells and the  
290 injection step of the mutant ES cells into the blastocysts<sup>45</sup>. The latest advances in  
291 genome editing tools can generate mutant mice within a single generation without the  
292 use of ES cells. Our crRNA (Crispr RNA) sequences designed *in silico*<sup>11,46</sup> are verified  
293 by *in vitro* Surveyor assay. They can be used to synthesize oligonucleotides as crRNA,  
294 which can be utilized for zygote injection. Our original protocol named “next-  
295 generation chromosome engineering” designed to target a specific chromosome locus  
296 of interest successfully generated mega-base scale CNVs of the chromosomal regions  
297 such as 3p14.1 (3.4 Mb), 3p26.3 (3.2 Mb), and 15q11-q13 (6.3 Mb).

298 Previous bulk transcriptome analyses identified converging biological  
299 processes and pathways of ASD<sup>35</sup>. A cell-type-specific study using patient samples  
300 suggested the importance of synaptic and neurodevelopmental genes in cortical upper  
301 layer 2/3 and clinical association with microglia<sup>29</sup>. In this study, using scRNA-seq  
302 analysis, we (1) identified CNV- and cell-type heterogeneity of ASD (17 cell-types  
303 from pathogenic 12 different CNVs); (2) confirmed the importance of synaptic, PSD  
304 complex, and neurodevelopmental genes on ASD pathogenesis; (3) showed that FMRP  
305 targets were enriched in neuronal cells, whereas CHD8 targets were broadly affected  
306 in various cells including non-neuronal cells, although both genes were ubiquitously  
307 expressed; (4) showed a significance of neuronal genes as upstream regulators; (5)  
308 identified enriched terms implicated in ASD, such as translation, transcriptional  
309 regulation, cell cycle, morphogenesis, and immune system; (6) showed two faces of  
310 ASD-associated CNVs, psychiatric and neurological disorders

311 Our isogenic cellular platform for ASD research can be extended for 3-  
312 dimensional culture organoid, imaging, and transplantation as well as drug screening.

313 In addition, our targeting and CRISPR/Cas9 vector collection and validated genome  
314 editing information could contribute to generating novel mouse models with CNVs.  
315 Our biological resource can be accessed through the web browser:  
316 <https://www.med.kobe-u.ac.jp/asddb/>  
317

318 **Acknowledgments**

319 We thank T. Yoshikawa and M. Toyoshima for the neural differentiation method, N.  
320 Mataga, K. Fukumoto, F. Sakai, N. Ito, C. Nishioka, M. Kadota and A. Kwon for  
321 experimental supports, Y. Okumura and M. Toki for database development, and all  
322 technical staff of the Takumi Lab for their technical assistance. This work was  
323 supported in part by KAKENHI (16H06316, 16H06463, 16F16110, 17K07119,  
324 21H00202, 21H04813, 21K07820, 21K19351) from Japan Society for the Promotion  
325 of Science (JSPS) and Ministry of Education, Culture, Sports, Science, and Technology,  
326 Japan Agency for Medical Research and Development (JP21wm0425011), Intramural  
327 Research Grant (30-9) for Neurological and Psychiatric Disorders of NCNP, Takeda  
328 Science Foundation, Smoking Research Foundation, SENSHIN Medical Research  
329 Foundation, Tokyo Biochemical Research Foundation, Research Foundation for Opto-  
330 Science and Technology, Hyogo Science and Technology Association, Kawano  
331 Masanori Memorial Public Interest Incorporated Foundation for Promotion of  
332 Pediatrics, Taiju Life Social Welfare Foundation, and Naito Foundation. AZ was  
333 supported by JSPS Postdoctoral Fellowship for Research in Japan.

334

335 **Author contributions**

336 J.N. and T.T. conceived and designed the study. T.T. supervised this project. J.N.  
337 drafted the manuscript. J.N. developed & implemented a chromosome manipulating  
338 technique. J.N., K.K., C.M., H.M., Y.N., Y.K., A.H., K.M., I.S., R.F., E.B., and K.Y.,  
339 developed ASD cell models and vector library. A.Z., K.F., H.M., Y.S., I.S., Y.N., K.K.,  
340 Y.K., C.M., N.N., and J.N. performed neural morphological and physiological  
341 experiments. T.A., E.T., J.N., K.K., C.M., Y.K., A.H., H.M., K.M., and K.Y., prepared  
342 ES cells for blastocyst injection and generated 15q13.3 chromosome mutant mice. J.N.,



343 M.S., Q.E., R.F., and C.M. performed behavioral tests. Y.K., C.M., and Y.N. performed  
344 cDNA library preparation. J.N., T.K., H.M., S.F., S.K., P.C., and J.S performed NGS  
345 and scRNA-seq analysis. J.N., H.M., Y.K., C.M., Y.N., A.H., K.K., K.M., R.F., X.L.,  
346 and T.T. developed ASD CNV database.  
347

## 348 **METHODS**

### 349 **Cell culture**

350 CMTI-2 mouse embryonic stem cell line (derived from murine strain C57BL/6J,  
351 normal male genotype, Millipore) and their derivatives were used for all experiments.  
352 mESCs were cultured in Dulbecco's modified Eagle's medium (DMEM, Gibco)  
353 supplemented with ES-qualified 15% FBS, 2 mM L-glutamine (Gibco), 0.1 mM MEM  
354 nonessential amino acids (NEAA, Gibco), nucleoside (Adenosine, Guanosine, Cytidine,  
355 Uridine, and Thymidine 30  $\mu$ M each, Sigma), 0.1 mM 2-mercaptoethanol (Sigma), and  
356 1,000 IU/ml LIF (ESGRO, Millipore) on mitomycin C-treated mouse embryonic  
357 fibroblasts (MEF) feeder cells. MEF cells were grown in Glasgow minimum essential  
358 medium (GMEM, Sigma) supplemented with 10% FBS.

359

### 360 **Establishment of ES cell lines from a blastocyst**

361 Preparation of 15q11-q13 mouse ES cells from blastocyst was established as previously  
362 described with some modification<sup>47</sup>. Briefly, fertilized embryos were collected from  
363 C57BL/6J female mice mated with 15q11-q13 duplication males for paternal 15q11-  
364 q13 duplication, or 15q11-q13 duplication female mice mated with C57BL/6J male  
365 mice for maternal 15q11-q13 duplication, respectively. The separated cells were  
366 transferred to the individual wells of 96 well plates coated with MEFs. ES cell  
367 establishment medium with 20% Knockout Serum Replacement (KSR; Invitrogen), 0.1  
368 mg/ml adrenocorticotrophic hormone (ACTH; fragments, American Peptide Company),  
369 instead of fetal bovine serum (FBS). After 10 days, proliferating outgrowths were  
370 dissociated and cultured until stable cell lines grew out.

371

### 372 **Vector construction**

373 CRISPR-Cas9 vectors for genome editing, pX330 (Addgene plasmid # 42230) was  
374 used. Annealed oligonucleotide for sgRNA was inserted into the BbsI site of pX330.  
375 Target sgRNAs were designed using the CRISPR design tool (<http://crispr.mit.edu/>) or  
376 CRISPRdirect (<https://crispr.dbcls.jp/>). To avoid off-target effects, only a higher score  
377 (>80; CRISPR design tool) or highly specific sequence (CRISPRdirect) were selected.  
378 The targeting vector cassette (DT-A/Neo #09, RIKEN BDR) contains a neomycin  
379 resistance gene and a DT-A cassette to avoid random integration. 5' and 3' homology  
380 arms were inserted into the outside of the neomycin resistance gene cassette in this  
381 vector. Target-specific crRNA sequence and primer set to make homology arms for  
382 targeting vectors are listed in Supplementary Table 2. All clones used in this study are  
383 available from RIKEN Bioresource Center, Japan (BRC, Gene engineering division:  
384 <https://dna.brc.riken.jp/en/>).

385

### 386 **Chromosome manipulation in mouse ES cells**

387 The donor targeting vector was linearized by Asp718 (Roche). Mouse ES cells, CMTI-  
388 2 (Millipore), were electroporated using the Nucleofector II (Lonza). Program #A-23  
389 was used for all electroporation. In each experiment,  $5 \times 10^6$  trypsinized cells were  
390 resuspended in 93.5  $\mu$ l solution (mouse ES cell nucleofector kit, VPH-1001, Lonza).  
391 The solution includes 2  $\mu$ g of each CRISPR/Cas9 vector (4  $\mu$ g total) and 20  $\mu$ g of the  
392 linearized targeting vector. After mixing with the DNA solution, the suspension was  
393 transferred to cuvettes, and the vectors were quickly electroporated into the cells. On  
394 the second day post electroporation, 500  $\mu$ g/ml G418 (Nacalai Tesque) was applied to  
395 select neomycin-resistant ES cells, and each colony was cultured in a 96 well plate.  
396 Chromosome modification was verified by Southern blotting, PCR, quantitative RT-  
397 PCR, or array CGH.

398 Successfully targeted cell clones in this study are listed in Extended Data Table 4. All  
399 clones used in this study are available from RIKEN Bioresource Center, Japan (BRC,  
400 Cell engineering division: <https://cell.brc.riken.jp/en/>).

401

#### 402 **Array comparative genomic hybridization**

403 According to the manufacturer's protocol, the Array comparative genomic  
404 hybridization (aCGH) was performed using SurePrint G3 Mouse CGH Microarray Kit,  
405 1 x 1 M (Agilent Technologies). Genomic DNA from wild-type mouse ES cells (CMTI-  
406 2) was used as a reference. Signals were then analyzed using R.

407

#### 408 **Neural differentiation from mouse ES cells**

409 After being cultured on gelatin-coated dishes, mESCs were used to form an embryoid  
410 body. Cells were cultured on a nonadherent bacterial dish for 8 days in this suspension  
411 culture condition. Retinoic acid (5  $\mu$ M) was added on days 4 and 6, respectively<sup>48</sup>. After  
412 suspension culture, cells were dissociated and seeded onto the Poly-L-ornithine (PLO)  
413 and laminin-coated culture dish, and then started differentiation by using neuronal  
414 media including NeuroCult NSC Basal Medium (StemCell Technologies)  
415 supplemented with 2% (v/v) B27 (Life Technologies), 10 ng/ml brain-derived  
416 neurotrophic factor (R&D Systems), 10 ng/ml glial-derived neurotrophic factor (R&D  
417 Systems), 200  $\mu$ M ascorbic acid (Sigma-Aldrich) and 400  $\mu$ M dibutyryl-cAMP (Sigma-  
418 Aldrich)<sup>49</sup>. Typical neuronal morphology was observed within 2 days.

419

#### 420 **Immunocytochemistry and morphological analysis**

421 Differentiating neurons were transfected on day 1 with p $\beta$ actin-GFP by lipofectamine  
422 LTX and PLUS Reagent (Thermo Fisher Scientific) and cultured for additional 2 days

423 on laminin and PLO-coated glass coverslips. Immunocytochemical staining was  
424 performed on day 3. In this step, cells were fixed with 4% paraformaldehyde containing  
425 4% sucrose for 20 min at 37°C. After fixation, cells were washed twice with PBS for  
426 10 min. Then, cells were blocked with blocking buffer (2% goat serum, 1% Glycine,  
427 0.1% Poly-D-Lysine, 0.3% Triton, 1% BSA in PBS) for 1 h. Then, cells were incubated  
428 with primary antibody (mouse anti-GFP, 1:1000 dilution, Thermo Fisher Scientific) in  
429 blocking buffer in a humidified chamber overnight at 4 °C. The next day, cells were  
430 washed three times with PBS for 10 min and then incubated with the secondary  
431 antibody (goat anti-mouse Alexa 488, 1:1000 dilution, Thermo Fisher Scientific) in a  
432 blocking buffer for 1.5 h. After washing three times with PBS, nuclei were stained with  
433 DAPI (VECTOR Laboratories) for 10 min. Cells were then washed once with PBS for  
434 10 min and were mounted with FluorSave™ Reagent (Sigma-Aldrich) overnight at  
435 room temperature. All following steps were performed as described previously<sup>50</sup>.  
436 Images were taken by BZ-9000 (Keyence). Axon length, total neurite length, and the  
437 branch numbers were analyzed on WIS-Neuromath (Weizmann Institute of Science,  
438 Israel). Twenty neurons were randomly chosen.

439

#### 440 **Ca<sup>2+</sup> imaging**

441 Differentiated neurons were cultured on laminin and PLO-coated glass bottom-culture  
442 dish. The neurons cultured for 7-days on the dish were treated with 1 μM of the Ca<sup>2+</sup>-  
443 sensitive, membrane-permeable fluorescent dye Fluo-4-AM (Thermo Fisher Scientific)  
444 dissolved in recording buffer (135 mM NaCl, 5 mM KCl, 2 mM CaCl<sub>2</sub>, 2 mM MgCl<sub>2</sub>,  
445 10 mM HEPES, 10 mM glucose, at pH 7.4) for 30 min at 37 °C. After loading, cells  
446 were washed three times with the recording buffer at room temperature. Green  
447 fluorescence images were acquired using an EMCCD camera (iXon Ultra 897, Andor)

448 on a confocal microscope (IX81 FV1000, Olympus) through a 20× objective lens  
449 (Olympus) and 495-540 nm emission filters (Olympus). Time-lapse images of the  
450 neurons at room temperature were recorded for 24 s duration with 20 ms interval by  
451 MetaMorph (Molecular Devices). The neurons were stimulated by 25 mM KCl  
452 manually treated in the recording buffer at the middle time point of recoding (i.e., at 12  
453 s). Images from randomly selected 20 neurons were analyzed by Image J. Fluorescent  
454 intensities of the soma were averaged to represent the signal of the neuron  $F$ . This value  
455 was divided by the baseline signal value  $F_0$ , which was calculated as an average of  $F$   
456 before KCl treatment (i.e., 0 ~ 10 s), to obtain normalized fluorescence changes  $\Delta F/F$   
457 =  $(F-F_0)/F_0$ .

458

#### 459 **Southern blotting**

460 Genomic DNA (10  $\mu$ g) was digested with EcoRI for the 5' region and HindIII for the  
461 3' region, respectively. The digested DNA was electrophoresed on a 0.8% agarose gel  
462 and transferred to a Hybond-N+ membrane (GE Healthcare). The membrane was  
463 hybridized with a digoxigenin-labeled DNA probe generated with a PCR DIG Probe  
464 Synthesis Kit (Sigma). Hybridization with a 5' probe produced an 8.1 Kb band from  
465 the WT and a 5.1 Kb band from the targeted locus, while hybridized with a 3' probe  
466 produced a 12.4 Kb band from the WT and an 8.1 Kb band from the targeted locus.

467

#### 468 **Animals**

469 Mice were housed in a room with a 12-hour light/dark cycle (light on 8:00 a.m. and off  
470 8:00 p.m.) and provided *ad libitum* access to water and food. All protocols for animal  
471 experiments were approved by the Animal Care and Use Committees of the RIKEN  
472 Brain Science Institute and performed under the institutional guidelines and regulations.

473

#### 474 **Generation of 15q13.3 chromosome mutant mice**

475 To generate human 15q13.3 microdeletion model mice, C57BL/6 background ES cells  
476 with 15q13.3 heterozygote deletion were microinjected into BALB/c blastocysts. Then,  
477 sperm from the chimera mouse were fertilized *in vitro* (IVF) to generate 15q13.3(+/-)  
478 mice. Genotype was confirmed by Southern blot and three-primer PCR. PCR primer  
479 used for genotyping were as follows: L-Neo1, 5' -  
480 GTACTCGGATGGAAGCCGGTCTTGTC-3', 9\_15q13.3\_Wt\_Fw, 5'-  
481 ACGCAGGGTGTAGAAGCAAA-3', and 9\_15q13.3\_Wt\_Tg\_Rv, 5' -  
482 CCGGTCGATTGTGAGTTCA-3'.

483 PCR with 9\_15q13.3\_Wt\_Fw and 9\_15q13.3\_Wt\_Tg\_Rv primer pair produces a 395-  
484 bp fragment from the wild-type locus, whereas the L-Neo1 and 9\_15q13.3\_Wt\_Tg\_Rv  
485 primer pair have a 999-bp fragment from the targeted locus. PCR was performed with  
486 the Taq DNA Polymerase (NEB) following the manufacturer's protocol. The PCR  
487 program consisted of initial denaturation at 96°C for 1 min; 40 cycles of 96°C for 10 s,  
488 60°C for 10 s, and 68°C for 1 min.

489

#### 490 **RT-qPCR analysis**

491 Total RNA (0.5 µg) isolated from mouse cortices was subjected to reverse transcription  
492 (RT) with a SuperScript II Reverse Transcriptase (Thermo Fisher Scientific). The  
493 cDNA was subjected to quantitative PCR using SYBR Green PCR Master Mix  
494 (Applied Biosystems) and specific primers in a StepOnePlus (Applied Biosystems).  
495 PCR primer sequences (sense and antisense, respectively) were as follows: Chrna7, 5'-  
496 GCATGAAGACAGTCAGAGAAAGTAA -3' and 5'-  
497 CCCTGGCTTTGCTGGTATT -3'; Otud7a, 5'- TCTTCCTTCGCCTCATGC -3' and

498 5'- CACCTCCAGAGAGTGAGGAGTC -3'; and  $\beta$ -actin, 5'-  
499 TGGATGCCACAGGATTCCAT -3' and 5'- CGTGC GTGACATCAAAGAGAA -3'.

500 The amount of *Chrna7* and *Otud7a* were normalized using  $\beta$ -actin.

501

## 502 **Behavioral experimental design**

503 C57BL6/J strain mice older than 10 weeks were used for behavioral tests. In the cage,  
504 2-5 mice were housed together with littermates. Mice were maintained in a 12-h  
505 light/dark cycle (light on at 8:00) with *ad libitum* access to water and food. All  
506 behavioral tests were performed between 9:00 AM and 6:00 PM. Mice were habituated  
507 to the testing room for at least 30 min before starting the behavioral experiments to  
508 allow acclimatization.

509

## 510 **Open field test**

511 Locomotor activity was measured in the open field apparatus (50 x 50 x 30 cm, O'Hara)  
512 illuminated at 100 lux light for 1 hour. Total distance traveled, time spent in the center  
513 area, and the rearing were recorded using TimeOFCR4 (O'Hara). The center area was  
514 defined as 36% of the field.

515

## 516 **Y-maze spontaneous alternation test**

517 Spatial working memory was measured by the Y-maze test. The Y-maze apparatus  
518 consists of three arms. The apparatus was illuminated at 100 lux lights for 5 min. Each  
519 mouse was allowed to explore freely in the Y-maze in this test. The alternation rate was  
520 analyzed using TimeYM2 for Y-maze (O'Hara).

521

## 522 **Ultrasonic vocalization (USV)**



523 Postnatal day 6 (P6) pups were assessed for ultrasonic vocalization (USV). A pup  
524 separated from their mother and littermates was put into a plastic beaker (8 cm diameter,  
525 12 cm height, the bottom covered with gauze) with a condenser ultrasound microphone  
526 (CM16/CMPA, Avisoft Bioacoustics) and placed in a soundproof box. USVs were  
527 recorded for 5 min at a sampling rate of 250 kHz. The recorded data were analyzed  
528 using SASLab Pro (Avisoft Bioacoustics).

529

### 530 **Grooming**

531 Mice were placed in a clean, transparent plastic cage. The self-grooming behavior was  
532 recorded by a video camera for a 10 min test period following 10 min habituation. The  
533 amount of time spent self-grooming was counted using a stopwatch.

534

### 535 **Acoustic startle response**

536 Mice were placed in a Plexiglas cylinder and acclimated for 5 min. A test session was  
537 composed of 49 trials, and each trial was composed of prepulse sounds (0, 72, 74, 78,  
538 82, and 86 dB respectively) pulse - (120 dB) paired stimulus or a no prepulse - no pulse  
539 pair. The average acoustic startle response was calculated by no prepulse – 120 dB pair.

540

### 541 **Elevated plus maze test**

542 The elevated plus-maze apparatus (O'Hara) consists of two open arms (25 × 5 cm) and  
543 two enclosed arms of the same size with 15 cm high transparent walls. The arms and  
544 central square were made of white plastic plates and were elevated to a height of 55 cm  
545 above the floor. Mouse behavior was recorded during a 10 min test period. Anxiety-  
546 like behavior was measured by the percentage of time spent in the open arms. The maze  
547 was illuminated with 100 lux.

548

549 **Three-chamber social interaction test**

550 The testing apparatus consisted of a rectangular three-chamber box (O'Hara). Mice can  
551 move to each chamber (20 x 40 x 20 cm) through small square openings (5 x 3 cm).  
552 The apparatus was illuminated at 10 lux. This test consists of three sessions. The first  
553 session for habituation to the apparatus for 10 min. Then, an age-matched unfamiliar  
554 male mouse (C57BL/6J) was placed in the wire cage in one of the two side chambers,  
555 and the subject mouse was allowed to move freely in the test box for 10 min to assess  
556 sociability. Finally, a second unfamiliar male mouse (C57BL/6J) was placed in the wire  
557 cage at the other side of the chamber to assess social novelty. In this session, the  
558 previously used stranger mouse was considered a familiar mouse. The subject mouse  
559 was placed in the chamber and allowed to move freely in the test box for 10 min. Time  
560 spent in the area was analyzed using TimeCSI1 for the three-chamber social interaction  
561 test system (O'Hara).

562

563 **Flurothyl-induced seizures**

564 Flurothyl-induced seizure experiments were performed according to the previous  
565 study<sup>51</sup>. Briefly, the mice were placed individually in an air-tight glass chamber (2 L  
566 volume) in a ventilated chemical hood and then habituated to the chamber for 1 min.  
567 After habituation in a glass chamber, the mouse was exposed to 10% flurothyl  
568 (bis(2,2,2-trifluoroethyl) ether) in 95% ethanol. 10% Flurothyl solution was infused  
569 through a 5 ml syringe by using a microsyringe pump (KD Scientific) onto a gauze pad  
570 at the top of the chamber at a rate of 200  $\mu$ l/min. We analyzed seizure behaviors using  
571 a video camera. In the case of observation of a generalized seizure, we immediately

572 removed the lid of the chamber, exposing the mouse to fresh air to stop the seizure  
573 assay.

574

#### 575 **Single-cell cDNA library preparation and RNA-sequencing (scRNA-seq)**

576 Differentiated cells on day 15 (8 days suspension culture plus 7 days adherent culture)  
577 were harvested and dissociated using TrypLE Select (Gibco). Cells were then passed  
578 through a 20  $\mu$ m strainer and resuspended in 1 x PBS with 0.04% BSA buffer. Then,  
579 cell suspensions (concentration and viability were assessed using TC20 Automated Cell  
580 Counter (Bio-Rad)) were loaded on a Chromium Single Cell Controller (10x  
581 Genomics) to generate single-cell gel beads in emulsion (GEMs) by using Chromium  
582 Single Cell 3' Library and Gel Bead Kit v2 (10x Genomics) following the  
583 manufacture's introduction. Captured cells were lysed and the RNA was barcoded  
584 through reverse transcription in each GEM. Reverse-transcribed cDNAs were purified  
585 by using Myone DynaBeads. To ensure successful amplification and accurate  
586 concentration of cDNA, we used Agilent Bioanalyzer 2100 using a High Sensitivity  
587 DNA chip (Agilent). Post library construction quantification was performed by KAPA  
588 Library Quantification Kits (Roche) according to the manufacture's protocol.  
589 Sequencing was performed on an Illumina HiSeq 2000 or 1500 with pair-end using the  
590 following read length: 26 cycles Read1, 8 cycles i7 Index, and 98 cycles Read2.

591

#### 592 **Single-cell sequence data pre-processing**

593 The Illumina sequencer's base call files (BCLs) were demultiplexed and converted to  
594 sample-specific FASTQ files using the cellranger mkfastq pipeline. Then, raw reads  
595 were processed using cellranger count pipeline, which takes FASTQ files generated by  
596 cellranger mkfastq and performs alignment to the mouse reference data (mm10),

597 filtering, barcode counting, and Unique Molecular Identifier (UMI) counting. All  
598 scRNA-seq data were processed using R (v3.6.1). The datasets were processed  
599 following the pipeline of the Seurat (v3.0). Cells with unique feature counts of more  
600 than 2,500 or less than 200 and more than 5% mitochondrial counts were filtered out.  
601 Finally, a total of 14,396 cells (Ctrl, 1159; 1q21.1 dup, 969; 2p16.3, 655; 3q29, 738;  
602 7q11.23 dup, 907; 15q11.2, 357; 15q13.3, 987; 16p11.2, 996; 16p13.2, 1112; 17p11.2,  
603 750; 17q12, 2057; Xq27.3, 2361; Xq28, 1348 cells) were used for downstream analysis.  
604 The 13 datasets were integrated using the Seurat pipeline and performed dimensionality  
605 reduction for visualization by using Uniform Manifold Approximation and Projection  
606 (UMAP). For bulk analysis, cellranger aggr pipeline was used to identify each CNV's  
607 features by calculating each gene expression by 10x Genomics Loupe (TM) Cell  
608 Browser v.2.0.0 ([https://support.10xgenomics.com/single-cell-gene-](https://support.10xgenomics.com/single-cell-gene-expression/software/visualization/latest/what-is-loupe-cell-browser)  
609 [expression/software/visualization/latest/what-is-loupe-cell-browser](https://support.10xgenomics.com/single-cell-gene-expression/software/visualization/latest/what-is-loupe-cell-browser)).

610

### 611 **Gene ontology (GO) and pathway analysis**

612 Gene lists were submitted to the Metascape software  
613 (<http://metascape.org/gp/index.html#/main/step1>) for functional Annotation<sup>52</sup>.  
614 Enrichment terms from Biological Process (BP), Cellular Component (CC), and  
615 Molecular Function (MF) as GO analysis, as well as KEGG (Kyoto Encyclopedia of  
616 Genes and Genomes), were examined for further enrichment analysis. Enrichment  
617 network visualization was used to detect enriched term network. ToppFun software in  
618 the ToppGene Suite (<https://toppgene.cchmc.org/enrichment.jsp>)<sup>53</sup> was used to analyze  
619 DEGs to GWAS-based gene-disease associations. The Ingenuity Pathway Analysis  
620 (IPA: Qiagen Bioinformatics) was used for upstream and canonical pathway analysis.

621 SFARI genes and scoring modules were referred 06-20-2019 version of the SFARI  
622 database.

623

#### 624 **Statistics**

625 Statistical analysis was conducted using R, and data were analyzed using one-way  
626 analysis of variance (ANOVA), two-way repeated-measures ANOVA. Bonferroni  
627 correction was applied to multiple comparisons. The significance level was set to  $p <$   
628 0.05.

629

#### 630 **Data Availability**

631

#### 632 **References**

- 633 1. Lord, C., Elsabbagh, M., Baird, G. & Veenstra-Vanderweele, J. Autism  
634 spectrum disorder. *Lancet* **392**, 508–520 (2018).
- 635 2. De La Torre-Ubieta, L., Won, H., Stein, J. L. & Geschwind, D. H. Advancing  
636 the understanding of autism disease mechanisms through genetics. *Nat. Med.*  
637 **22**, 345–361 (2016).
- 638 3. Malhotra, D. & Sebat, J. CNVs: Harbingers of a Rare Variant Revolution in  
639 Psychiatric Genetics. *Cell* **148**, 1223–1241 (2012).
- 640 4. Takumi, T. & Tamada, K. CNV biology in neurodevelopmental disorders.  
641 *Curr. Opin. Neurobiol.* **48**, 183–192 (2018).
- 642 5. Basu, S. N., Kollu, R. & Banerjee-Basu, S. AutDB: A gene reference resource  
643 for autism research. *Nucleic Acids Res.* **37**, 832–836 (2009).
- 644 6. Abrahams, B. S. *et al.* SFARI Gene 2.0: a community-driven knowledgebase  
645 for the autism spectrum disorders (ASDs). *Mol. Autism* **4**, 36 (2013).

- 646 7. Marshall, C. R. *et al.* Contribution of copy number variants to schizophrenia  
647 from a genome-wide study of 41,321 subjects. *Nat. Genet.* **49**, 27–35 (2017).
- 648 8. Green, E. K. *et al.* Copy number variation in bipolar disorder. *Mol. Psychiatry*  
649 **21**, 89–93 (2016).
- 650 9. Chang, A. N. *et al.* Neural blastocyst complementation enables mouse  
651 forebrain organogenesis. *Nature* **563**, 126–130 (2018).
- 652 10. Kendall, K. M. *et al.* Association of Rare Copy Number Variants with Risk of  
653 Depression. *JAMA Psychiatry* **76**, 818–825 (2019).
- 654 11. Cong, L. *et al.* Multiplex genome engineering using CRISPR/Cas systems.  
655 *Science (80-. )*. **339**, 819–823 (2013).
- 656 12. Liu, X. *et al.* Sequence features associated with the cleavage efficiency of  
657 CRISPR/Cas9 system. *Sci. Rep.* **6**, 1–9 (2016).
- 658 13. Nakatani, J. *et al.* Abnormal Behavior in a Chromosome- Engineered Mouse  
659 Model for Human 15q11-13 Duplication Seen in Autism. *Cell* **137**, 1235–1246  
660 (2009).
- 661 14. Fejgin, K. *et al.* A Mouse Model that Recapitulates Cardinal Features of the  
662 15q13.3 Microdeletion Syndrome Including Schizophrenia- and Epilepsy-  
663 Related Alterations. *Biol. Psychiatry* **76**, 128–137 (2014).
- 664 15. Kogan, J. H. *et al.* Mouse Model of Chromosome 15q13.3 Microdeletion  
665 Syndrome Demonstrates Features Related to Autism Spectrum Disorder. *J.*  
666 *Neurosci.* **35**, 16282–16294 (2015).
- 667 16. Sanders, S. J. *et al.* Insights into Autism Spectrum Disorder Genomic  
668 Architecture and Biology from 71 Risk Loci. *Neuron* **87**, 1215–1233 (2015).

- 669 17. Leppa, V. M. M. *et al.* Rare Inherited and De Novo CNVs Reveal Complex  
670 Contributions to ASD Risk in Multiplex Families. *Am. J. Hum. Genet.* **99**, 540–  
671 554 (2016).
- 672 18. Sztainberg, Y. & Zoghbi, H. Y. Lessons learned from studying syndromic  
673 autism spectrum disorders. *Nat. Neurosci.* **19**, 1408–1418 (2016).
- 674 19. Baba, M. *et al.* Psychiatric-disorder-related behavioral phenotypes and cortical  
675 hyperactivity in a mouse model of 3q29 deletion syndrome.  
676 *Neuropsychopharmacology* **44**, 2125–2135 (2019).
- 677 20. Artegiani, B. *et al.* A Single-Cell RNA Sequencing Study Reveals Cellular and  
678 Molecular Dynamics of the Hippocampal Neurogenic Niche. *Cell Rep.* **21**,  
679 3271–3284 (2017).
- 680 21. Saunders, A. *et al.* Molecular Diversity and Specializations among the Cells of  
681 the Adult Mouse Brain. *Cell* **174**, 1015-1030.e16 (2018).
- 682 22. Zeisel, A. *et al.* Molecular Architecture of the Mouse Nervous System. *Cell*  
683 **174**, 999-1014.e22 (2018).
- 684 23. Zhang, Y. *et al.* An RNA-sequencing transcriptome and splicing database of  
685 glia, neurons, and vascular cells of the cerebral cortex. *J. Neurosci.* **34**, 11929–  
686 11947 (2014).
- 687 24. Zeng, H. *et al.* Large-scale cellular-resolution gene profiling in human  
688 neocortex reveals species-specific molecular signatures. *Cell* **149**, 483–496  
689 (2012).
- 690 25. Shrestha, P., Mousa, A. & Heintz, N. Layer 2/3 pyramidal cells in the medial  
691 prefrontal cortex moderate stress induced depressive behaviors. *Elife* **4**, 1–24  
692 (2015).

- 693 26. Tremblay, R., Lee, S. & Rudy, B. GABAergic Interneurons in the Neocortex:  
694 From Cellular Properties to Circuits. *Neuron* **91**, 260–292 (2016).
- 695 27. Karagiannis, A. *et al.* Classification of NPY-expressing neocortical  
696 interneurons. *J. Neurosci.* **29**, 3642–3659 (2009).
- 697 28. Dougherty, J. D., Schmidt, E. F., Nakajima, M. & Heintz, N. Analytical  
698 approaches to RNA profiling data for the identification of genes enriched in  
699 specific cells. *Nucleic Acids Res.* **38**, 4218–4230 (2010).
- 700 29. Velmeshev, D. *et al.* Single-cell genomics identifies cell type-specific  
701 molecular changes in autism. *Science (80-. ).* **364**, 685–689 (2019).
- 702 30. Schafer, S. T. *et al.* Pathological priming causes developmental gene network  
703 heterochronicity in autistic subject-derived neurons. *Nat. Neurosci.* **22**, 243–  
704 255 (2019).
- 705 31. Zhan, Y. *et al.* Deficient neuron-microglia signaling results in impaired  
706 functional brain connectivity and social behavior. *Nat. Neurosci.* **17**, 400–6  
707 (2014).
- 708 32. Salter, M. W. & Stevens, B. Microglia emerge as central players in brain  
709 disease. *Nat. Med.* **23**, 1018–1027 (2017).
- 710 33. Ouellette, J. *et al.* Vascular contributions to 16p11.2 deletion autism syndrome  
711 modeled in mice. *Nat. Neurosci.* **23**, 1090–1101 (2020).
- 712 34. Voineagu, I. *et al.* Transcriptomic analysis of autistic brain reveals convergent  
713 molecular pathology. *Nature* **474**, 380–384 (2011).
- 714 35. Quesnel-Vallières, M., Weatheritt, R. J., Cordes, S. P. & Blencowe, B. J.  
715 Autism spectrum disorder: insights into convergent mechanisms from  
716 transcriptomics. *Nat. Rev. Genet.* **20**, 51–63 (2019).



- 717 36. Marchetto, M. C. *et al.* Altered proliferation and networks in neural cells  
718 derived from idiopathic autistic individuals. *Mol. Psychiatry* **22**, 820–835  
719 (2017).
- 720 37. Masi, A. *et al.* Cytokine aberrations in autism spectrum disorder: A systematic  
721 review and meta-analysis. *Mol. Psychiatry* **20**, 440–446 (2015).
- 722 38. Rossignol, D. A. & Frye, R. E. A review of research trends in physiological  
723 abnormalities in autism spectrum disorders: Immune dysregulation,  
724 inflammation, oxidative stress, mitochondrial dysfunction and environmental  
725 toxicant exposures. *Mol. Psychiatry* **17**, 389–401 (2012).
- 726 39. Lee, P. H. *et al.* Genomic Relationships, Novel Loci, and Pleiotropic  
727 Mechanisms across Eight Psychiatric Disorders. *Cell* **179**, 1469–1482.e11  
728 (2019).
- 729 40. Bourgeron, T. From the genetic architecture to synaptic plasticity in autism  
730 spectrum disorder. *Nat. Rev. Neurosci.* **16**, 551–563 (2015).
- 731 41. Forrest, M. P., Parnell, E. & Penzes, P. Dendritic structural plasticity and  
732 neuropsychiatric disease. *Nat. Rev. Neurosci.* **19**, 215–234 (2018).
- 733 42. Bayés, Á. *et al.* Characterization of the proteome, diseases and evolution of the  
734 human postsynaptic density. *Nat. Neurosci.* **14**, 19–21 (2011).
- 735 43. Levine, A. J. P53: 800 Million Years of Evolution and 40 Years of Discovery.  
736 *Nat. Rev. Cancer* **20**, 471–480 (2020).
- 737 44. Krishnan, A. *et al.* Genome-wide prediction and functional characterization of  
738 the genetic basis of autism spectrum disorder. *Nat. Neurosci.* **19**, 1454–1462  
739 (2016).

- 740 45. Wang, H. *et al.* One-step generation of mice carrying mutations in multiple  
741 genes by CRISPR/cas-mediated genome engineering. *Cell* **153**, 910–918  
742 (2013).
- 743 46. Naito, Y., Hino, K., Bono, H. & Ui-Tei, K. CRISPRdirect: Software for  
744 designing CRISPR/Cas guide RNA with reduced off-target sites.  
745 *Bioinformatics* **31**, 1120–1123 (2015).
- 746 47. Wakayama, S. *et al.* Efficient Establishment of Mouse Embryonic Stem Cell  
747 Lines from Single Blastomeres and Polar Bodies. *Stem Cells* **25**, 986–993  
748 (2007).
- 749 48. Bibel, M. *et al.* Differentiation of mouse embryonic stem cells into a defined  
750 neuronal lineage. *Nat. Neurosci.* **7**, 1003–1009 (2004).
- 751 49. Toyoshima, M. *et al.* Analysis of induced pluripotent stem cells carrying  
752 22q11.2 deletion. *Transl. Psychiatry* **6**, e934-10 (2016).
- 753 50. Nakanishi, M. *et al.* Functional significance of rare neuroligin 1 variants found  
754 in autism. *PLoS Genet.* **13**, 1–28 (2017).
- 755 51. Judson, M. C. C. *et al.* GABAergic Neuron-Specific Loss of Ube3a Causes  
756 Angelman Syndrome-Like EEG Abnormalities and Enhances Seizure  
757 Susceptibility. *Neuron* **90**, 56–69 (2016).
- 758 52. Zhou, Y. *et al.* Metascape provides a biologist-oriented resource for the  
759 analysis of systems-level datasets. *Nat. Commun.* **10**, 1523 (2019).
- 760 53. Chen, J., Bardes, E. E., Aronow, B. J. & Jegga, A. G. ToppGene Suite for gene  
761 list enrichment analysis and candidate gene prioritization. *Nucleic Acids Res.*  
762 **37**, 305–311 (2009).
- 763
- 764

765 **Figure legend**

766 **Figure 1. ASD cell bank for functional analysis**

767 **a**, Schematic diagram to generate a cellular model of ASD with chromosomal  
768 abnormalities, and strategy to identify ASD-associated pathogenic phenotypes using  
769 representative ASD cell lines. **b**, Representative image of chromosome targeting locus  
770 in mouse chromosome 7 (7qC) corresponds to human 15q13.3 locus. **c**, Schematic of  
771 the sgRNA targeting sites in *Chrna7* and *Otud7a*, respectively. The target sequences  
772 are underlined and labeled in blue. The protospacer adjacent motif (PAM) sequence is  
773 underlined and labeled in red. **d**, Structures of the mouse 7qC genomic locus, the  
774 targeting vector, and the targeted locus mediated by genome editing technique. The  
775 restriction enzymes used for Southern blotting analysis are shown. The targeting vector  
776 contains the PGK-neo-pA cassette with diphtheria toxin A-fragment (DT-A) for  
777 positive and negative selection. The 5' and 3' probes are shown as red and blue boxes,  
778 respectively. EcoRI-digested genomic DNA was hybridized with a 5' probe to produce  
779 an 8.1 kb band from wild-type (WT) and a 5.1 kb band from the targeted locus. HindIII-  
780 digested genomic DNA was hybridized with a 3' probe to produce a 12.4 kb band from  
781 WT and an 8.3 kb from the targeted locus. **e**. Targeted mouse chromosome loci  
782 corresponding to human ASD-associated chromosome loci.

783

784 **Figure 2. Transcriptional features and heterogeneity of cells harboring ASD-**  
785 **associated CNVs.**

786 **a**. UMAP dimensionality reduction embedding of differentiated neurons and the  
787 derivatives from mouse ES cells harboring ASD-associated CNVs. Whole cells were  
788 colored by annotated cell types. **b**. Feature plots of characteristic marker genes for the  
789 cell types are shown. Cells are color-coded according to gene expression levels. **c**.

790 Heatmaps show the expression pattern of cell-type-specific genes. Columns represent  
791 individual cells, and rows represent individual genes. The representative differentially  
792 expressed genes are listed to the right. **d.** Violin plot showing the expression profile of  
793 each gene in various cell types. **e.** Cell-type-specific Expression Analysis (CSEA) using  
794 each glutamatergic or GABAergic cell-cluster-specific genes (top 300 independent  
795 genes,  $q < 0.001$ ). It highlights the brain area with the development period in each  
796 neuronal cluster. **f.** The number of overlapping genes between genetic risk factors  
797 (SFARI genes, risk score 1, 2, 3, and syndromic genes) and cell-type-specific DEGs  
798 (top 300 genes,  $q < 0.001$ ) in each cell cluster. Color-coding is consistent with **(a and**  
799 **c).** **g.** Network visualization of enriched terms. The network is visualized using  
800 Metascape and Cytoscape. Each node represents an enriched GO/pathway term and is  
801 colored by their p-values. Edges link similar terms.

802

803 **Figure 3. Cell-type and CNV- specific pathway analysis.**

804 **a.** Heatmap for the cell-type-specific enriched canonical pathways was performed by  
805 using Ingenuity Canonical Pathways Analysis. Each column in the figure represents an  
806 ASD-associated CNV, and each row represents a canonical pathway. The colors in the  
807 graph indicate the  $-\log_{10}(\text{p-value})$ . **b.** Cell-type-specific single-cell RNA-seq data were  
808 used for the analysis. Numbers of DEGs and proportion of genes involved in major  
809 targets of ASD (SFARI ASD risk genes, FMRP targets, CHD8 targets, members of  
810 WNT  $\beta$ -catenin pathway, and members of MAP kinase pathway, respectively) were  
811 analyzed.

812

813

814

815 **Extended data figures and tables**

816 **Extended Data Figure 1. Generation and characterization of mice mimicking**

817 **human 15q13.3 microdeletion syndrome**

818 **a.** Mouse C57/BL6J strain CMTI-2 ES cell line with chromosome 7 (7qC)

819 heterozygote deletion were grown on mitotically inactive primary mouse embryonic

820 fibroblasts (MEF) were injected into 3.5-day old blastocysts and implanted into

821 pseudo-pregnant BALB/c female mice. Chimera rate was determined by coat color. **b.**

822 Male chimera mice with an approximately 60% coat color contribution of CMTI-2 ES

823 cells. **c.** Genotypes of ES cells determined by PCR. PCR with the three primers

824 produces a 395-bp band from the wild-type (WT) and a 999-bp band from the

825 targeted locus. **d.** Quantitative real-time PCR (qRT-PCR) analysis. Total RNA was

826 purified from male adult WT and 15q13.3 (+/-) mouse cortices, respectively.

827 Expression level of *Chrna7* and *Otud7a* were normalized by  $\beta$ -actin.  $n = 3$

828 mice/genotype were used for the analysis. Both *Chrna7* and *Otud7a* expression levels

829 were significantly reduced in 15q13.3(+/-), *Chrna7*,  $F(1,4) = 27.344$ ,  $p < 0.01$ ;

830 *Otud7a*,  $F(1,4) = 21.577$ ,  $p < 0.01$  **e.** Body weights growth curves of WT and

831 15q13(+/-) mice. In the test period, significant difference was observed between two

832 genotypes.  $F(1, 285) = 4.453$ ,  $p < 0.0357$ , two-way repeated ANOVA (WT,  $n = 30$ ;

833 15q13.3(+/-),  $n = 29$ ). **f.** Brain weights were assessed at 5 months age. No significant

834 difference was observed between WT and 15q13.3(+/-).  $F(1, 19) = 0.17$ ,  $p = 0.685$ ,

835 one-way ANOVA ( $n = 3$  for each genotype). **g.** Open field test to analyze locomotor

836 activity, anxiety, vertical activity in the novel environment. There is no significant

837 difference between genotypes, total distance,  $F(1,38) = 0.203$ ,  $p = 0.655$ ; percentage

838 of time spent in the center area,  $F(1,38) = 0.066$ ,  $p = 0.799$ ; and the number of rearing

839 in the open field chamber,  $F(1,38) = 0.188$ ,  $p = 0.667$  ( $n = 20$  for each genotype). **h.**

840 Spontaneous alternation Y-maze test to analyze spatial working memory. There is no  
841 significant difference between genotypes,  $F(1,38) = 1.174$ ,  $p = 0.285$  ( $n = 20$  for each  
842 genotype). **i.** Ultrasonic vocalization test (USV) to analyze an early communicative  
843 behavior between mother and their dams. There is no significant difference between  
844 genotypes,  $F(1,68) = 0.527$ ,  $p = 0.47$  (WT,  $n = 36$ ; 15q13.3(+/-),  $n = 34$ ). **j.** Grooming  
845 number was counted to analyze core autistic symptoms (e.g. repetitive and excessive  
846 self-grooming). There is no significant difference between genotypes,  $F(1,42) =$   
847  $0.052$ ,  $p = 0.82$  ( $n = 20$  for each genotype). **k.** Acoustic startle response was assessed  
848 to see an exaggerated startle response to an unexpected auditory stimulus. Startle  
849 response was significantly increased in 15q13.3(+/-) mice.  $F(1,38) = 5.622$ ,  $p < 0.05$   
850 ( $n = 20$  for each genotype). **l.** Elevated plus maze test was performed to analyze  
851 anxiety-like behavior. There is no significant difference between genotypes,  $F(1,38) =$   
852  $0.098$ ,  $p = 0.756$ ,  $F(1,38) = 0.219$ ,  $p = 0.642$ , closed and opened arms respectively ( $n$   
853  $= 20$  for each genotype). **m.** Three-chamber social interaction test to assess  
854 sociability. Both ctrl and 15q13.3(+/-) mice significantly stay longer in stranger cage  
855 than empty cage,  $F(1,32) = 8.21$ ,  $p < 0.01$ ,  $F(1,38) = 48.69$ ,  $p < 0.01$ , respectively.  
856 Although ctrl mice stay longer in stranger mice than familiar mice area,  $F(1,32) =$   
857  $4.602$ ,  $p < 0.05$ , no significant difference was observed in 15q13.3(+/-) mice,  $F(1,38)$   
858  $= 0.448$ ,  $p = 0.507$  (WT,  $n = 17$ ; 15q13.3(+/-),  $n = 20$ ). **n.** Schematic of GABA<sub>A</sub>R  
859 antagonist, flurothyl-induced seizure protocol and experimental setting. **o.** Latency to  
860 generalized seizure were analyzed in both genotypes and genders. Two-way ANOVA  
861 revealed no significant main effect of genotype ( $F(1, 52) = 0.073$ ,  $p = 0.78$ ) and  
862 gender ( $F(1,52) = 0.113$ ,  $p = 0.738$ ), and no significant interaction between genotype  
863 and gender ( $F(1, 52) = 3.08$ ,  $p = 0.085$ ) (Male WT,  $n = 9$ ; male 15q13.3(+/-),  $n = 14$ ;  
864 female WT,  $n = 17$ ; female 15q13.3(+/-),  $n = 16$ ). **p.** Frequency of generalized seizure

865 were analyzed in both genotypes and genders. Two-way ANOVA revealed significant  
866 main effect of genotype ( $F(1, 52) = 4.923, p < 0.05$ ), but not in gender ( $F(1,52) =$   
867  $0.004, p = 0.95$ ) (Male WT,  $n = 9$ ; male 15q13.3(+/-),  $n = 14$ ; female WT,  $n = 17$ ;  
868 female 15q13.3(+/-),  $n = 16$ ).

869

870 **Extended Data Figure 2. Analyzed targeted deletion or duplication of the cellular**  
871 **model of ASD by array-CGH**

872 Genomic DNA was extracted from control and twelve representative mutant mouse  
873 ES cells, respectively. Control genomic DNA was used as a reference. Each dot  
874 represents an oligonucleotide. A red shaded region indicates a deleted or duplicated  
875 region. Analysis was designed by referring to the mouse reference sequence mm9  
876 (NCBI Build 37).

877

878 **Extended Data Figure 3. Morphological and physiological analyses of neurons**  
879 **derived from mES cells.**

880 **a, b, c, d.** Box plots of the axon length (**a**), total neurite length (**b**), and total branch  
881 number (**c**) in mouse ESC-derived neurons, respectively. (total  $n=1348$  cells  
882 including;  $n=179$  (Ctrl); 75 (1q21.1 dup); 82 (2p16.3); 155 (3q29); 69 (7q11.23 dup);  
883  $n=79$  (15q11.2); 160 (15q13.3); 92 (16p11.2); 65 (16p13.2); 71 (17p11.2); 82  
884 (17q12); 85 (Xq27.3); 154 (Xq28)). **d.** Traces show the relative change in  
885 fluorescence intensity ( $\Delta F/F$ ) induced by 25 mM KCl at day 3. **e.** The averaged peak  
886 amplitude of  $Ca^{2+}$  response ( $\Delta F/F$ ) was evoked by 25 mM KCl. Box plots show  
887 median, quartiles (boxes), and range (whiskers). P-values are determined by One-  
888 way-ANOVA with post hoc Bonferroni multiple comparison test (**a, b, c, e**). \*\*\* $p <$   
889 0.001.

890

891 **Extended Data Figure 4. Functional and Molecular signature of ASD-associated**  
892 **CNVs.**

893 **a-c.** Gene ontology (GO) analysis for clustering of CNVs. Biological Process (BP)(**a**),  
894 Molecular Function (MF)(**b**), and Cellular Component (CC)(**c**), respectively. The  
895 rows of the heatmap represent the GO terms and the columns represent CNVs. **d.**  
896 Canonical pathway analysis was performed by using Ingenuity Canonical Pathways  
897 Analysis. The rows of the heatmap are the canonical pathway and the columns  
898 indicate CNVs. The gradient of color in the heatmap indicates the enrichment levels.  
899 The heatmap color indicates statistical significance ( $-\text{Log}_{10}(\text{p-value})$ ).

900

901 **Extended Data Figure 5. Gene-disease association analysis identified psychiatric**  
902 **and neurological aspects of ASD-associated CNVs.**

903 The heatmap shows the interaction between neuropsychiatric, neurological disorders,  
904 and ASD-associated CNVs in a cell-type-specific manner. The rows of the heatmap  
905 are the major psychiatric and neurological disorders, and the columns are ASD-  
906 associated CNVs. The red line indicates a member of the psychiatric disorders, while  
907 the green line indicates a member of neurological disorders. The gradient of color in  
908 the heatmap indicates the enrichment levels. The heatmap color indicates statistical  
909 significance ( $-\text{Log}_{10}(\text{p-value})$ ).

910

911 **Extended Data Figure 6. Significance of the glutamatergic postsynaptic density**  
912 **genes and upstream regulator in ASD.**

913 **a.** Overlap between glutamatergic (*Slc17a6*<sup>+</sup>) cell-cluster (Figure 2b, #8 and #10)  
914 specific DEGs and postsynaptic density (PSD) genes. The X-axis represents the



915 number of DEGs in each cell cluster and Y-axis represents glutamatergic neuronal  
916 cells clusters in each CNV. The red column indicates PSD complex genes. SFARI  
917 genes (gene scores 1 to 3 and syndromic) in each DEGs are listed to the right. The  
918 numbers in parentheses indicate the risk gene score of ASD defined by SFARI, and  
919 genes without score indicate a syndromic gene. **b. Cell-type-specific upstream-**  
920 **regulators.** The numbers in parentheses indicate the risk gene score defined by  
921 SFARI, and genes without a score are not SFARI ASD risk genes. The rows of the  
922 heatmap are the upstream regulator genes, and columns are CNVs. The gradient of  
923 color in the heatmap indicates the enrichment levels. The heatmap color indicates  
924 statistical significance (-Log<sub>10</sub>(p-value)).

925

926

927 **Extended Data Table 1. Major CNVs associated with ASD.**

928 **Extended Data Table 2. Common CNVs among psychiatric disorders (targeted**  
929 **CNVs in the study)**

930 **Extended Data Table 3. Common genes among psychiatric disorders (target**  
931 **CNVs in our study).**

932 **Extended Data Table 4. Cell library.**

933 **Extended Data Table 5. Consequence of chromosome targeting.**

934 **Extended Data Table 6. Synteny analysis (targeted CNVs).**

935 **Extended Data Table 7. Gene expression in targeted loci.**

936 Gene expression of each cell-line. Genes located in targeted region were analyzed.

937 Average expression, logFC, p-value were derived from scRNA-seq data. P-values

938 were adjusted using the Benjamini-Hochberg correction for multiple tests. \*p < 0.1,

939 \*\*p < 0.05, \*\*\*p < 0.01, \*\*\*\*p < 0.001.

940 **Extended Data Table 8. Cell-type (cluster) specific Gene Ontology (GO) terms.**

941 **Extended Data Table 9. Gene Ontology analysis; ASD associated 12 CNVs.**

942

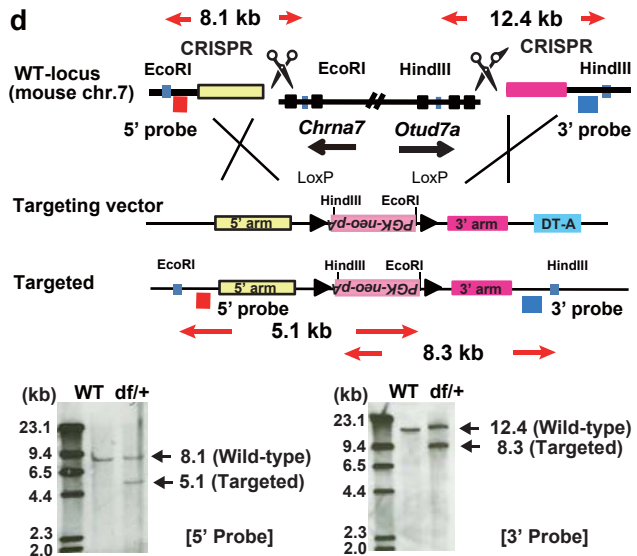
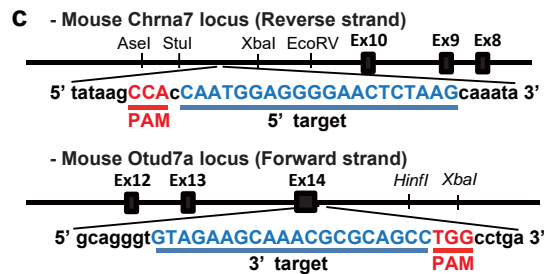
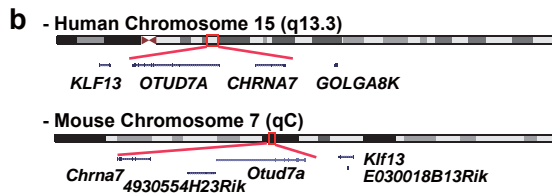
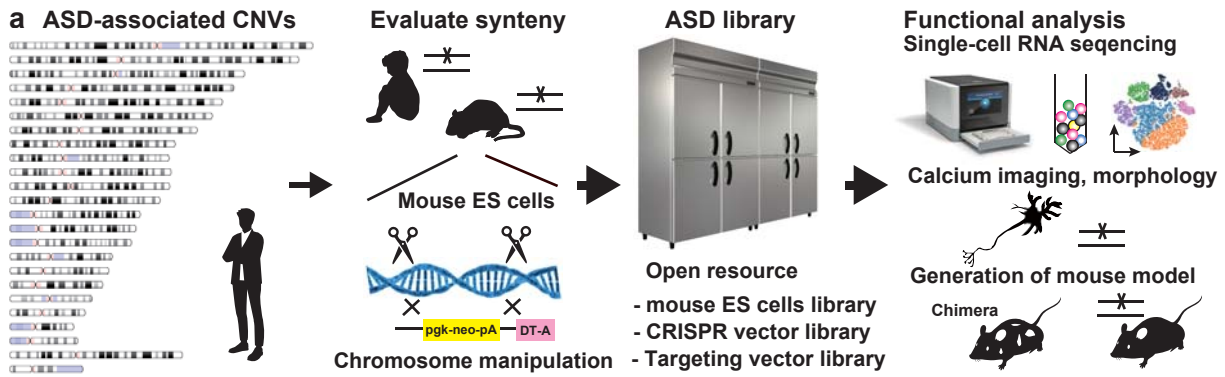
943 **Supplementary Table 1. Synteny analysis; low syntenic CNV.**

944 **Supplementary Table 2. CRISPR and targeting vectors used in the study.**

945 **Supplementary Table 3. Cell-type markers in each cell cluster.**

946

**Figure 1**

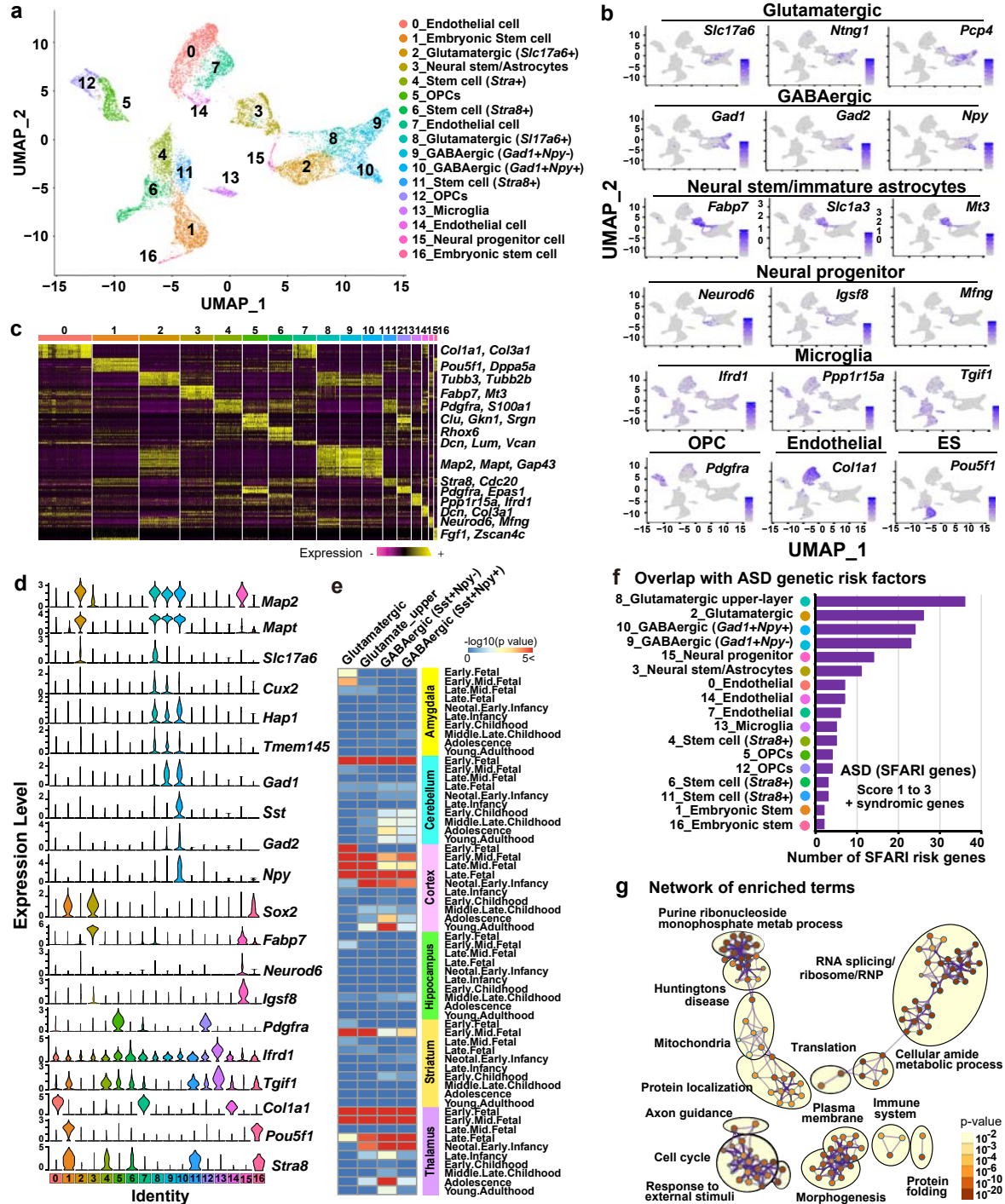


**e**

Human chr	Human CNV locus	Mouse chr	Length (Kb)	CNV type
1	1q21.1	3	805.5	del/+
1	1q21.1	3	805.5	dup/+
1	1q25.3	1	1398.7	del/+
2	2p16.3	17	1059.4	del/+
2	2p21	17	673.3	del/+
2	2p22.3	17	864.2	del/+
2	2p25.3	12	1431.8	del/+
3	3p12.3	16	1748.7	del/+
3	3p14.1	6	3409.6	del/+
3	3p14.2	14	1611.9	del/+
3	3p26.3	6	3289.5	del/+
3	3q29	16	1210.5	del/+
4	4p16.3	5	462.3	del/+
4	4p16.3	5	336.1	del/+
4	4q13.2	5	601.1	del/+
4	4q28.3	3	1069.8	del/+
5	5p15.33	13	124.4	del/+
6	6p12.3	17	903.3	dup/+
6	6p25.3	13	314.0	del/+
6	6q26	17	1223.0	del/+
6	6q27	17	721.3	del/+
7	7p21.1	12	956.9	del/+
7	7q11.22	5	1106.0	del/+
7	7q11.23	5	731.8	del/+
7	7q11.23	5	731.8	dup/+
7	7q11.23	5	1130.2	del/+
7	7q31.1	12	1509.5	del/+
7	7q35	6	1081.4	del/+
8	8p22	8	2093.8	del/+
8	8p23.1	8	1318.6	del/+
8	8p23.1	14	1468.8	del/+
10	10q21.3	10	1573.6	del/+
11	11p13	2	1577.1	del/+
12	12p13.33	6	609.2	del/+
14	14q32.33	12	1696.9	del/+
15	15q11.2	7	225.8	del/+
15	15q11.2	14	39.6	del/+
15	15q11.2-q13.1	7	6369.9	del/+
15*	15q11.2-q13.1 (paternal)	7	6369.9	dup/+
15*	15q11.2-q13.1 (maternal)	7	6369.9	dup/+
15	15q13.1-q13.2	7	1026.1	del/+
15	15q13.2-q13.3	7	1293.5	del/+
15	15q13.3	7	660.3	del/+
15	15q14	7	2081.7	del/+
15	15q25.2-25.3	7	473.6	del/+
16	16p11.2	7	438.1	del/+
16	16p11.2	7	438.1	dup/-
16	16p12.1	7	347.1	del/+
16	16p13.11	16	234.6	del/+
16	16p13.11	16	572.6	del/+
16	16p13.2	16	603.3	del/+
16	16p13.2	16	603.3	dup/-
16	16p13.2	16	513.1	del/+
16	16q23.1	8	3903.9	del/+
16	16q23.3	8	1767.1	del/+
17	17p11.2	11	1127.0	del/+
17	17p12	11	971.1	del/+
17	17p13.1	11	777.0	del/+
17	17q12	11	1066.3	del/+
20	20p12.1	2	1997.7	del/+
20	20q13.33	2	1268.2	del/+
22	22q11.21	16	1408.4	del/+
22	22q13.33	15	701.3	del/+
x	Xq27.3	X	39.4	del/y
x	Xq28	X	108.8	del/y

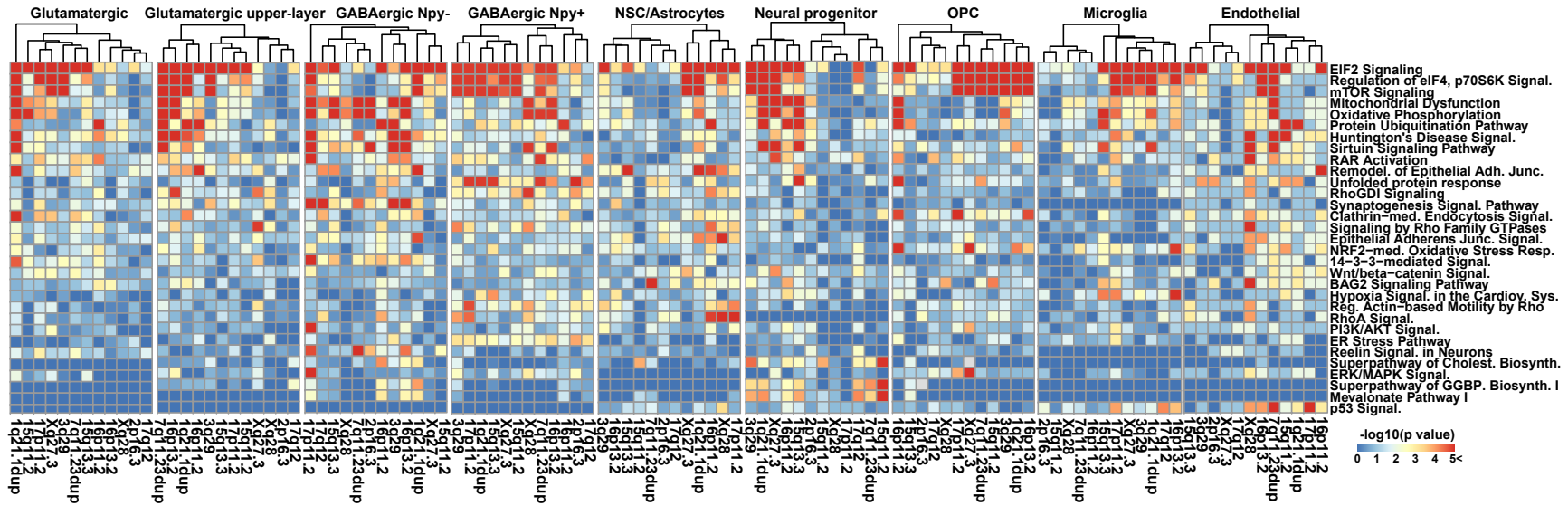
ES Cells were established from mouse blastocyst.

Figure 2



**Figure 3**

**a. Canonical pathway**



**b. Major targets of ASD**

